Raman scattering and photoluminescence of ZnS_xTe_{1-x} mixed crystals

1998 J. Phys.: Condens. Matter 10 4119

(http://iopscience.iop.org/0953-8984/10/18/021)

J. Phys.: Condens. Matter **10** (1998) 4119–4129. Printed in the UK PII: S0953-8984(98)87498-5

Raman scattering and photoluminescence of ZnS_xTe_{1-x} mixed crystals

N Z Liu†, G H Li†, Z M Zhu†, H X Han†, Z P Wang†, W K Ge‡ and I K Sou‡

† National Laboratory for Superlattices and Microstructures, Institute of Semiconductors, Academia Sinica, Beijing 100083, People's Republic of China

‡ Department of Physics, Hong Kong University of Science and Technology, Clear Water Bay, Kowloon, Hong Kong

Received 9 September 1997, in final form 13 January 1998

Abstract. We have investigated the Raman scattering and the photoluminescence (PL) of ZnS_xTe_{1-x} mixed crystals grown by MBE, covering the entire composition range ($0 \leqslant x < 1$). The results of Raman studies show that the ZnS_xTe_{1-x} mixed crystals display two-mode behaviour. In addition, photoluminescence spectra obtained in backscattering and edge-emission geometries, reflectivity spectra and the temperature dependence of the photoluminescence of ZnS_xTe_{1-x} have been employed to find out the origin of PL emissions in ZnS_xTe_{1-x} with different x values. The results indicate that emission bands, for the samples with small x values, can be related to the band gap transitions or a shallow-level emission centre, while as x approaches 1, they are designated to strong radiative recombination of Te isoelectronic centres (IECs).

1. Introduction

Wide-band-gap II–VI semiconductors have attracted increasing interest for they have a great potential for visible light-emitting devices in the blue–green region. Studies on II–VI epilayers and quantum well heterostructures containing Te showed that Te acted as an isoelectronic centre [1, 2] that strongly enhances the luminescence intensity of the parent II–VI materials. Moreover, Te atoms may form single point defects (Te_1 centres) and Te_n ($n \geqslant 2$) clusters [3–5] to explain the spectral features in the II–VI semiconductors.

The room-temperature band gap energy of the ZnS_xTe_{1-x} mixed crystal spans the entire visible and near-UV range (2.26 to 3.60 eV), making it a promising candidate for an optoelectronic as well as blue–green light-emitting device. It also enjoys the advantage that it can be lattice-matched to ZnSe, GaAs and InP, as well as Si substrates. However, compared to some other II–VI mixed crystals such as ZnSeTe [6, 7], ZnS_xTe_{1-x} mixed crystals are relatively unexplored. Most of the previous studies of ZnS_xTe_{1-x} mixed crystals prepared by electron beam evaporation [8, 9], radio frequency sputtering [10, 11], metalorganic vapour phase epitaxy (MOVPE) [12] and molecular beam epitaxy (MBE) [13] were mainly concerned with the composition dependence of its lattice constant and band gap. Two recent works reported the room-temperature PL [13] and Raman studies [14] of ZnS_xTe_{1-x} mixed crystals.

In present article, we report a further study on the optical properties of ZnS_xTe_{1-x} mixed crystals. We have studied the Raman scattering and the photoluminescence of ZnS_xTe_{1-x}

0953-8984/98/184119+11$19.50

mixed crystals grown by MBE, over the whole composition range. Results of Raman scattering demonstrate that the optical phonons of ZnS_xTe_{1-x} mixed crystals exhibit two-mode behaviour. The PL of ZnS_xTe_{1-x} with different composition is studied at 10 K. Peak energies are close to the band gap for the samples with low-S composition, but the energies recede from the band gap as we move toward high-S composition. Reflectivity spectra as well as the temperature dependence of the photoluminescence show that near-band-edge emission dominates in the small-x region and emission by strong radiative recombination of the Te isoelectronic centre dominates in the large-x region

2. Samples and experiments

The samples used in this study were grown by the MBE technique in a VG V80H system. Semi-insulating GaAs(001) substrates with $2^\circ \pm 0.1^\circ$ off toward the $\langle 011 \rangle$ direction were used. ZnS_xTe_{1-x} mixed crystals were grown using compound ZnS and ZnTe sources contained in separate effusion cells. Te composition was controlled by adjusting the cell temperatures. As Te composition increased from $x = 0$ to $x = 1$, the optimal growth temperature increased from 160 to 300 °C. The thickness of the epilayers measured by optical reflectivity technique spans from 0.52 to 2.9 μm. The strain in the alloy layer has been relaxed. The composition of ZnS_xTe_{1-x} films was determined using energy dispersive x-ray spectrometry carried out in an EDAX DX-4 system. The accuracy of Te composition was within 0.01. The detailed sample parameters are summarized in table 1.

Table 1. The composition of S (x), thickness, Raman shifts, PL energy (E_{PL}), the sum of PL energy and activation energy ($E_{PL} + \varepsilon$), and integrated PL intensity (I).

Samples	x	Thickness (μm)	ZnTe-like mode (cm^{-1})	ZnS-like mode (cm^{-1})	E_{PL} (eV)	$E_{PL} + \varepsilon$ (eV)	I (count s^{-1} eV)
1	0.00	2.9	206.5		2.375		1.2×10^4
2	0.02		206.6		2.317	2.365	6.8×10^4
3	0.04	0.52	205.5		2.260		1.3×10^4
4	0.15	1.8	206.6	282.8	2.193	2.226	1.0×10^6
5	0.25	1.4	197.1	291.8	2.136	2.173	2.1×10^6
6	0.29	1.3	196.0	297.4	2.128	2.166	2.0×10^6
7	0.53	1.5	198.8	314.2	2.143	2.226	1.1×10^7
8	0.70	0.36	206.6	323.1	2.210	2.336	1.4×10^7
9	0.79	1.6		331.0	2.297	2.441	2.9×10^7
10	0.92	2.8		339.9	2.537		3.4×10^7
11	0.98	1.85			2.715		1.5×10^4
12	0.99	0.97			2.721		1.1×10^4

Raman scattering was carried out in a back-scattering geometry at room temperature. The 413.1 nm line of a Kr^+ laser was used as the source of excitation. The scattered light was dispersed by a Jobin–Yvon T64000 triple monochromator and detected by a liquid nitrogen cooled CCD. The low-temperature PL measurements were performed by fixing the samples on the cold finger of a DE-202 type refrigeration system. The temperature can be varied from 10 to 300 K. The 413.1 nm line of a Kr^+ laser was used as the source of excitation. The emitted light is dispersed by a Jobin–Yvon HRD-2 double monochromator and detected by a cooled photomultiplier with GaAs cathode. We carried out PL measurements in the back-scattering and edge-emission geometries. In edge-emission mode, the emission is detected from the cleaved edge of the sample. In this geometry, we can eliminate the optical interference effects.

3. Results and discussion

3.1. Raman scattering

The simple mass criterion derived form the MREI (modified random element isodisplacement) model [15, 16] predicts that the ZnS_xTe_{1-x} mixed crystal should possess two-mode behaviour because the mass of the substituting element (S) is smaller than the reduced mass of the compound formed by the other two elements (ZnTe). Figure 1 shows the Raman spectra of ZnS_xTe_{1-x} mixed crystal samples with different composition. The Raman shifts of each of them are shown in table 1. There are two types of vibrational mode in ZnS_xTe_{1-x} ternaries. Similar results were reported by Jin *et al* [14] who used the 488.0 nm line as the source of excitation. The composition dependences of vibrational mode frequencies obtained from Raman spectra are plotted in figure 2. The solid lines represent the results of least-squares fits to the experimental data using a linear relation. The extrapolation of the fitting curve shows that at the end compositions ($x = 0$ and 1), the frequency of one mode is very close to the local mode of S in ZnTe (278 cm^{-1} [15]) and the LO (longitudinal optical) phonon mode of pure ZnS (348 cm^{-1} [16]), respectively, while the other one comes very close to the LO phonon mode of pure ZnTe (205 cm^{-1} [15]) at $x = 0$, and the gap mode of Te in ZnS (200 cm^{-1} [16]) at $x = 1$. So we identify the former as ZnS-like LO phonons and the latter at around 205 cm^{-1} are from ZnTe-like LO phonons. This assignment can be proved by the composition dependence of these two modes. The ZnTe-like LO phonon mode dominates the Raman spectra of samples with low S compositions, while samples with higher S compositions show the dominant feature

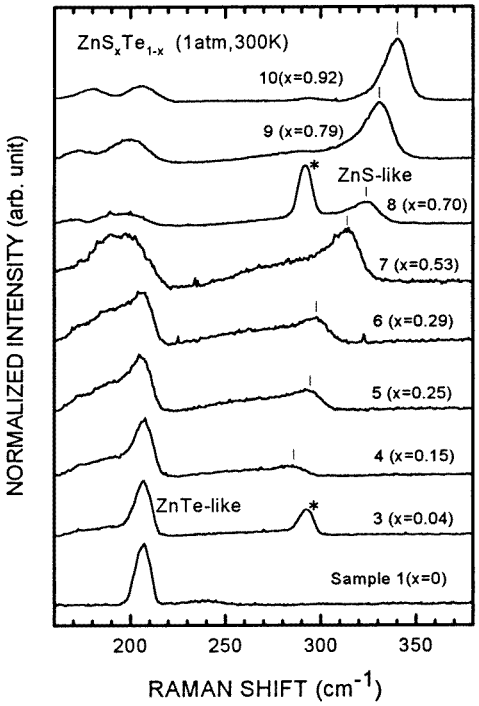

Figure 1. Raman scattering of the ZnS_xTe_{1-x} samples. The intensities have been normalized according to the respective strongest peak.

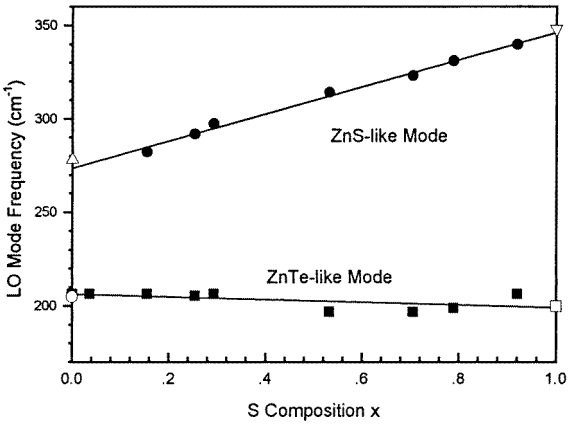

Figure 2. The frequencies of ZnTe-like LO phonon mode (■) and ZnS-like LO phonon mode (●) in ZnS_xTe_{1-x} as a function of S composition x. The solid lines represent the least-squares fits using a linear relation. △ represents the local mode of S in ZnTe, ▽ represents the LO phonon mode of pure ZnS, ○ represents the LO phonon mode of pure ZnTe, □ represents the gap mode of Te in ZnS.

of the ZnS-like mode. The relative intensity of the ZnS-like mode to the ZnTe-like mode increases as the S composition increases. The frequency of the ZnS-like mode shows a remarkable linear shift from 280 to 348 cm^{-1} as the S composition increases, whereas the ZnTe-like mode shifts only slightly in the entire composition range. In the spectra of sample 3 ($x = 0.04$) and sample 8 ($x = 0.70$), the peaks labelled * at 292.0 cm^{-1}, which are absent from other samples, are believed to be originated from the LO phonons of the GaAs substrate [17] mainly due to the very small thickness of the ZnSTe epilayers of these two samples. A weak peak on the lower-energy side of the ZnTe-like mode is assigned to the ZnTe-like TO (transverse optical) phonon [14]. The appearance of the TO phonon in the spectra is attributed to the relaxation of the q conservation law in the scattering process that is due to alloy disorder [18]. In this case, the Raman shift of the LO mode is obtained from the curve fitting process. In the samples with x approaching 1, we observed a peak at about 180 cm^{-1}. The origin of this peak is still not very clear.

3.2. Low-temperature photoluminescence

The PL spectra of ZnS_xTe_{1-x} samples for various x obtained at 10 K are shown by solid lines in figure 3. In the PL spectrum of pure ZnTe ($x = 0$), two near-band-edge emission peaks at 2.375 eV and 2.358 eV are dominant. The higher-energy one can be assigned as emission from bound exciton transition [19, 20]. The lower one is the first LO phonon replica of free-exciton transition. For sample 2 ($x = 0.02$) and sample 3 ($x = 0.04$), PL spectra mainly show two emission features. The higher-energy peak is most likely from free-to-bound (FB) transitions. The lower-energy peak carrying the PL properties of a donor–acceptor pair (DAP) can be interpreted as an emission originating from an IEC (isoelectronic centre) acceptor pair (IAP) [21]. The PL spectra of samples 4 ($x = 0.15$), 5 ($x = 0.25$) and 6 ($x = 0.29$) are dominated by a narrow emission peak. A relatively broader emission band is dominant in the PL spectra of samples 7 ($x = 0.53$), 8 ($x = 0.70$), 9 ($x = 0.79$), 10 ($x = 0.92$), 11 ($x = 0.98$) and 12 ($x = 0.99$). The line width of the emission peaks increases as S composition increases. As S composition approaches 1

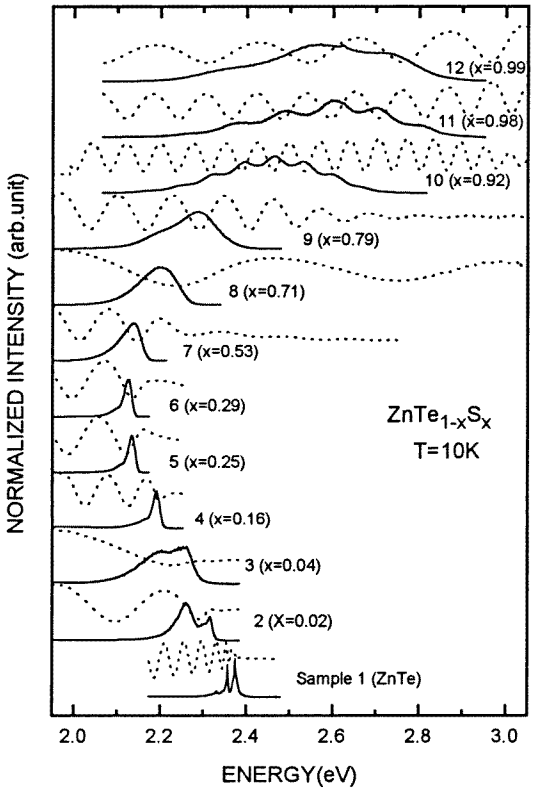

Figure 3. PL spectra (solid line) and reflection spectra (dotted line) of ZnS_xTe_{1-x} at 10 K. The intensities have been normalized according to the respective strongest peak.

(samples 10–12), the PL peaks show regular periodic oscillations in intensity which are also observed in previous work [13].

Reflectivity measurements were undertaken to find out the origin of the period oscillations. The reflectivity spectra of each sample are depicted by dotted lines in figure 3. The comparison between the reflectivity spectra and PL spectra of samples 10 ($x = 0.92$), 11 ($x = 0.98$) and 12 ($x = 0.99$) shows that the period of the regular periodic oscillations in intensity is equal to the period of the reflection spectra. Thus, the spectral oscillations are due to optical interference effects.

It is known that the intensity of reflectivity spectra of thin-film crystals varies only slightly in the range of energies higher than the band-edge but shows period oscillations owning to the optical interference effects in the range of energies lower than the band-edge. By comparing the PL spectra with the reflectivity spectra we found that the PL energy is near the band edges in the samples with low S compositions ($x < 0.3$), while in the samples with high S compositions ($0.3 < x < 1$) the PL energy is remarkably lower than the band edges.

In order to obtain precise positions of the PL peaks of samples 10 ($x = 0.92$), 11 ($x = 0.98$) and 12 ($x = 0.99$), we tried carrying out PL measurements in an edge-emission geometry. As an example, figure 4(c) shows the PL spectrum of sample 10 ($x = 0.92$) obtained in the edge-emission mode (as depicted in the illustrative scheme on the right).

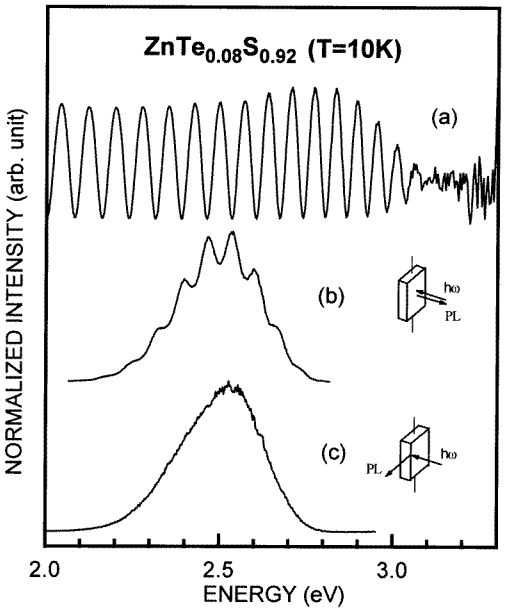

Figure 4. (a) Reflection spectra, (b) PL spectra obtained in standard backscattering geometry and (c) PL spectra in edge-emission mode (as depicted in the illustrative scheme on the right) of sample 10 obtained at 10 K.

Here, the exciting light is focused on the sample surface, the emission is detected from the cleaved edge of the sample. Reflectivity and PL spectra in the conventional backscattering geometry are also shown in figure 4(a) and (b) respectively for a comparison. It can be seen clearly that by using edge-emission mode we can successfully eliminate the regular periodic oscillations in intensity. It is also shown more clearly that the period oscillations come from the optical interference effects.

Peak positions of PL spectra obtained at 10 K are summarized in table 1 and compared with the band gaps at the corresponding sulphur composition, as shown in figure 5. The peak positions of samples 7 ($x = 0.53$), 8 ($x = 0.70$), 9 ($x = 0.79$), 10 ($x = 0.92$), 11 ($x = 0.98$) and 12 ($x = 0.99$) are obtained in edge-emission mode. For samples 1 ($x = 0$), 2 ($x = 0.02$), 3 ($x = 0.04$), 4 ($x = 0.15$), 5 ($x = 0.25$) and 6 ($x = 0.29$), the peak positions are obtained in back-scattering mode. The interference effects in these samples can be neglected because the PL energies are near the absorption band edges. The shifting trend of the PL peak is similar to the previous results obtained at room temperature [13]. The line is the band gap energy described by

$$E_g(x) = E_A + (E_B - E_A - b)x + bx^2 \tag{1}$$

where b is 3.0 eV found experimentally [9], E_A and E_B are the band-gap energies of pure ZnTe and ZnS compound semiconductor, respectively. Different experimental values of E_A and E_B are reported [22]; average values are taken as 2.392 and 3.83 eV, respectively, for reference. For small values of x, the PL emission energy is close to the band gap, indicating that the main radiative centre of the mixed crystal is a shallow one. For large values of x, the E_{PL} is much smaller than the band gap, indicating that the transition involves a relatively deep centre.

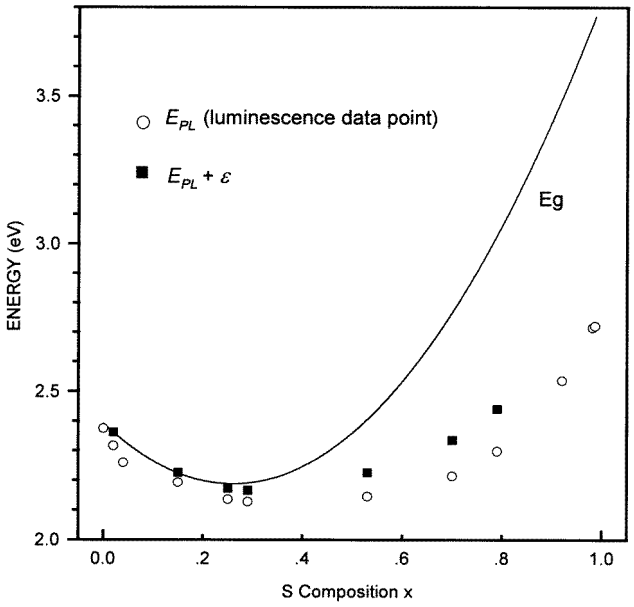

Figure 5. The composition dependence of luminescence peak energy at 10 K compared with band gap energy (solid line) described by (1).

Iseler and Strauss [23] have reported the observation of two emission peaks associated with Te traps in ZnS. The high-energy peak at 3.1 eV was related to a single Te atom (Te_1), and the low-energy one at 2.7 eV to paired Te atoms (Te_2) on the nearest-neighbour sites. Only the Te_1 emission band can be observed in low-Te-concentration samples, and Te_2 in the higher one [3]. In higher-Te-concentration (>3.0%) samples, a emission band found at 2.55 eV was ascribed to the radiative annihilation of excitons bound to the Te_3 cluster [4]. In our experiments, a broad emission peak at about 2.7 eV was found in samples 11 ($x = 0.98$) and 12 ($x = 0.99$). We attributed it to emission from excitons bound to Te_2 pairs. In sample 10 ($x = 0.92$), we found a emission peak at 2.54 eV, which can be attributed to the radiative annihilation of excitons bound to a Te_3 cluster.

3.3. Temperature dependence

PL spectra of eight ZnS_xTe_{1-x} samples were taken over a temperature range from 10 to 290 K. The results presented in figure 6 show the spectra of two samples obtained at different temperatures. It can be seen that an increase in temperature leads to a redshift of PL energy.

The experimental temperature dependence of PL energy of samples 1 (ZnTe), 2 ($x = 0.02$), 4 ($x = 0.15$), 5 ($x = 0.25$), 7 ($x = 0.53$), 8 ($x = 0.70$), 9 ($x = 0.79$) and 11 ($x = 0.98$) is shown in figure 7. The temperature dependence of the direct band gap can be described by a 'Bose–Einstein' type expression [24]:

$$E_0(T) = E_0(0) - 2a_B/[\exp(\theta_B/T) - 1] \tag{2}$$

where $E_0(0)$ is the band gap at $T = 0$ K, a_B represents the strength of the electron (exciton)–average phonon interaction and θ_B corresponds to the average phonon temperature.

The experimental data of sample 1 (ZnTe) plotted in solid circles can be satisfactorily fitted to (2) with ($a_B = 0.0371$, $\theta_B = 155.0$) as shown in figure 7. The solid line shows

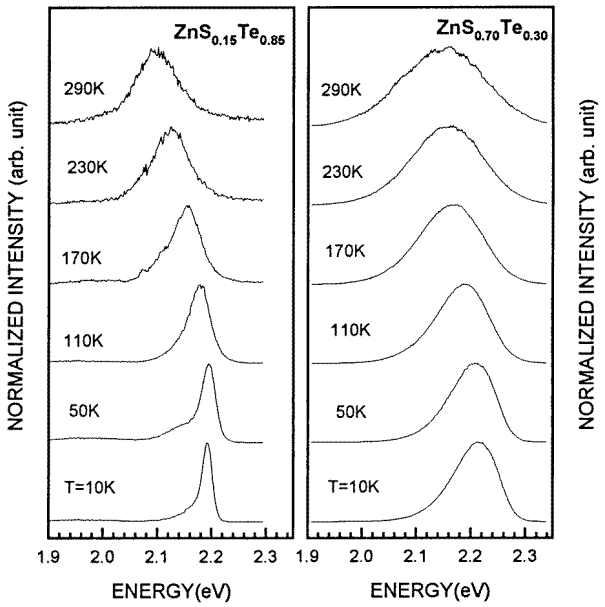

Figure 6. PL spectra obtained over a temperature range from 10 K to 290 K. PL intensity is normalized to its maximum peak intensity.

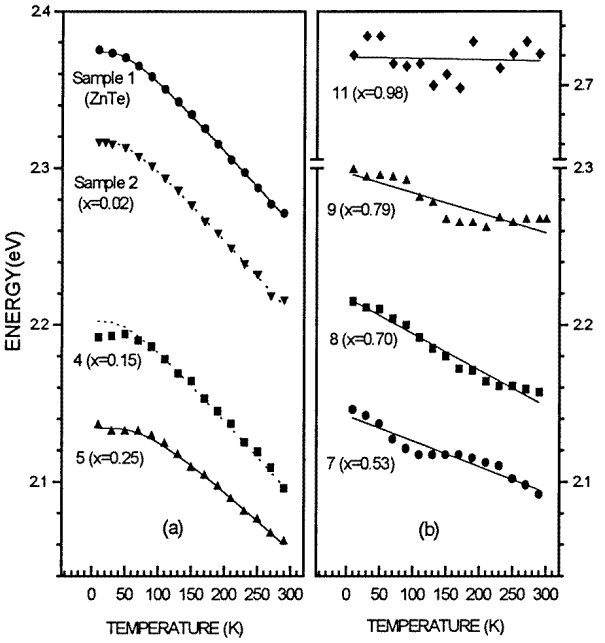

Figure 7. (a) The experimental temperature dependence of PL peak energy of ZnS_xTe_{1-x} samples with low S compositions. The solid lines are the least-squares fit to the data points described by (2). The dotted lines are the results of vertically shifting the fitting curve of sample 1. (b) The experimental temperature dependence of PL peak energy of ZnS_xTe_{1-x} samples with high S compositions. The solid lines are the least-squares fit to the data points using a linear relation.

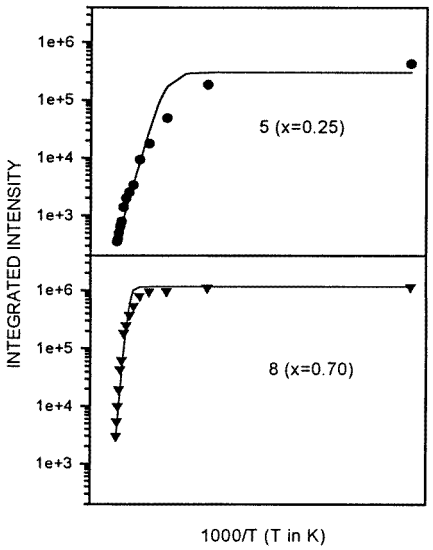

Figure 8. Temperature dependence of PL intensity of samples 5 and 8. The solid line shows the fitting curve described by (3).

the least-squares fitting curve described by (2). It is found that the temperature dependence of samples 2 ($x = 0.02$) and 4 ($x = 0.15$) is similar to that of ZnTe. The peak shifting of samples 2 ($x = 0.02$) and 4 ($x = 0.15$) can be well fitted by vertically shifting the fitting curve of ZnTe. Dotted lines are plotted for the results of the vertical shifting. The peak shifting trend of sample 5 ($x = 0.25$) can also be fitted by (2) but the parameters are different ($a_B = 0.0499$, $\theta_B = 247.8$). These results imply that the PL peaks of samples with low S compositions can be associated with the band gap or a shallow-level emission centre. For samples 7 ($x = 0.53$), 8 ($x = 0.70$), 9 ($x = 0.79$) and 11 ($x = 0.98$), the emission energy shifts much more slowly with temperature than that of ZnTe; especially, when the value of x approaches 1 ($0.8 < x < 1$), the energy varies only slightly. The solid line shows the least-squares fit to the data points using a linear relation. These observations indicate that PL emission from a deep-level centre dominates in these samples.

The temperature dependence of the integral PL intensity of two ZnS_xTe_{1-x} mixed crystals is shown in figure 8. The PL intensity is exponentially reduced in the higher-temperature region, mainly due to thermally activated nonradiative recombination mechanisms. This luminescence quenching is characterized by a relatively high activation energy. Based on a simple model, the temperature dependence of the PL intensity can be expressed by the equation [23]:

$$I(T) = I(0) \Big/ \left\{1 + s \exp\left(-\frac{\varepsilon}{kT}\right)\right\} . \tag{3}$$

The term $s \exp(-\varepsilon/kT)$ is the probability of nonradiative transition. ε represents the activation energy for the internal thermal quenching. The thermal quenching of the PL emission in the high-temperature region is fitted by linear regression for estimating the activation energies ε. The solid lines in figure 8 represent the fitting curve described by (3). (Peak intensity became weaker in sample 3 ($x = 0.04$) and almost undetectable at high temperature. In sample 10 ($x = 0.92$), 11 ($x = 0.98$) and 12 ($x = 0.99$), peak intensity varies only slightly as the temperature increase, so we cannot obtain the activation

energy of these samples.) The sums of activation energy ε and E_{PL} are shown in table 1. The sums of ε and E_{PL} plotted in solid squares are compared with the band-gap energy in figure 5. It can be seen that in the low-S-composition range ($x < 0.3$), the energy is approximately the same as the band edge after adding ε to E_{PL}. Here, carriers were excited from a shallow impurity state to the band-edge, which lead to the exponential decrease of PL intensity as temperature increases. Therefore, the activation energy ε obtained in this region is regarded as the binding energy of the shallow impurity. However, in the range with higher S compositions ($0.3 < x < 0.8$), the energy is still much lower than the band gap even after ε is added, which indicates that the activation energies we obtained in this region are not the binding energies of the impurity. Perhaps the active energies obtained represent the transition of the electrons from the measured energy level to a higher energy level. Further research is under way in our laboratory.

4. Conclusion

Raman scattering, photoluminescence in backscattering and edge-emission geometries, reflectivity measurements and temperature dependence of the PL of ZnS_xTe_{1-x} have been investigated in our work. The results demonstrate that the ZnS_xTe_{1-x} mixed crystals display two-mode behaviour. The frequency of the ZnS-like mode shows a remarkable shift toward 351 cm^{-1} (the frequency of the ZnS LO phonon) as the S content increases, whereas the ZnTe-like mode shifts only slightly over the entire composition range. By use edge-emission mode, we successfully eliminate the regular periodic oscillations in intensity in PL spectra and obtain precise peak positions. Low-temperature PL and temperature dependence of the PL show that the emission of ZnS_xTe_{1-x} with small x value ($x < 0.3$) can be related to the band gap or a shallow-level emission centre, while in the region with very large x ($0.8 < x < 1$) the emission comes from a deep-level centre—the Te isoelectronic centre.

Acknowledgment

The project was supported by the National Natural Science Foundation of China.

References

[1] Lee D, Mysyrowicz A, Nurmikko A V and Fitzpatrick B J 1987 *Phys. Rev. Lett.* **58** 1475
[2] Fu Q, Lee D, Nurmikko A V, Kolodziejski L A and Gunshor R L 1989 *Phys. Rev.* B **39** 3137
[3] Fukushima T and Shionoya S 1973 *Japan. J. Appl. Phys.* **12** 549
[4] Heimbrodt W and Goede O 1986 *Phys. Status Solidi* b **135** 795
[5] Hoshina T and Kawai H 1980 *Japan. J. Appl. Phys.* **19** 279
[6] Yao T, Kato M, Davies J J and Tanino H 1988 *J. Cryst. Growth* **86** 552
[7] Reznitsky A, Permogorov S, Verbin S, Naumov A, Korostelin Y, Novozhilov V and Prokovev S 1984 *Solid State Commun.* **52** 13
[8] Hill R and Richardson D 1973 *Thin Solid Films* **15** 303
[9] Hill R and Richardson D 1973 *J. Phys. C: Solid State Phys.* **6** L115
[10] Tokumitsu Y, Kitayama H, Kawabuchi A, Imura T and Oska Y 1989 *Japan. J. Appl. Phys.* **28** 345
[11] Tokumitsu Y, Kitayama H, Kawabuchi A, Imura T and Oska Y 1990 *J. Cryst. Growth* **99** 455
[12] Yokogawa T and Narusawa T 1992 *J. Cryst. Growth* **117** 480
[13] Sou I K, Wong K S, Yang Z Y, Wang H and Wong G K L 1995 *Appl. Phys. Lett.* **66** 1915
[14] Jin C X, Ling Z, Huang D M, Hou X Y and Wang Xun 1997 *J. Appl. Phys.* **81** 3465
[15] Peterson D L, Petrou A, Giriat W, Ramdas A K, and Rodriguez S 1986 *Phys. Rev.* B **33** 1160
[16] Chang I F and Mitra S S 1986 *Phys. Rev.* **72** 942
[17] Pizani P S, Mlayah A, Groenen J, Carles R and Claverie A 1995 *Appl. Phys. Lett.* **66** 1972

[18] Cardona M 1982 *Light Scattering in Solid II* ed M Cardona and G Guntherodt (Heidelberg: Springer) p 9
[19] Feldman R D, Austin R F, Bridenbaugh P M, Johnson A M, Simpson W M, Wilson B A and Bonner C E 1988 *J. Appl. Phys.* **64** 1198
[20] Wilson B A, Bonner C E, Feldman R D, Austin R F, Kisker D W, Krajewski J J and Bridenbaugh P M 1988 *J. Appl. Phys.* **64** 3210
[21] Lam S B, Sou I K, Ge W K, Li G H, Han H X and Wang Z P 1997 *Phys. Rev.* B **55** 10 035
[22] *Landolt–Bornstein New Series* 1982 vol 17b (Berlin: Springer)
[23] Iseler G W and Strauss A J 1970 *J. Lumin.* **3** 1
[24] Lautenschlager P, Garriga M, Logothetidis S and Cardona M 1987 *Phys. Rev.* B **35** 9174